Contribution from the Sohio Research Center,
Cleveland, Ohio 44128

Stabilization of High-Temperature Antimony Oxide with Molybdenum Incorporation. Structure of Mo-Doped Sb_2O_4 by Powder Neutron Diffraction and Extended X-ray Absorption Fine Structure Spectroscopy

RAYMOND G. TELLER,* MARK R. ANTONIO, JAMES F. BRAZDIL, M. MEHICIC, and ROBERT K. GRASSELLI

Received September 25, 1984

It has been discovered that the presence of MoO_3 lowers the α-β transition in Sb_2O_4 from 935 to 850 °C with concurrent dissolution of Mo in the high-temperature (β) form. The structure of Mo-doped β-Sb_2O_4 has been investigated by powder neutron diffraction, extended X-ray absorption fine structure (EXAFS) and Raman spectroscopies, and scanning-electron microscopy (SEM). Cell parameters: a = 12.0571 (12) Å, b = 4.8335 (1) Å, c = 5.3838 (6) Å, β = 105.579 (5)°, monoclinic, space group $C2/c$, Z = 4. Combining the results of these techniques leads to the hypothesis that Mo is located interstitially within channels of electron density in the Sb_2O_4 structure with concurrent vacancy of two Sb^{III} atoms. There is no apparent oxygen deficiency in the resulting structure.

Introduction

In view of the importance of molybdenum and antimony oxides in heterogeneous catalysis,[1] it is surprising that only within the last decade have there been significant additions to the MoO_3–Sb_2O_4 phase diagram. Parmentier et al. have postulated the existence of two discrete compounds, Sb_2MoO_6 and $Sb_2Mo_3O_{12}$, in the phase diagram.[2] The existence of the former phase has been firmly established by a powder neutron diffraction profile analysis,[3] whereas compelling evidence for the stoichiometry of the latter phase is lacking. In more recent work, Parmentier et al. have synthesized materials of the formulas $Sb_{0.2}MoO_{3.1}$ and $Sb_{0.4}MoO_{3.1}$,[4] both of which bear some resemblance to molybdenum bronzes.

Due to its multivalent nature, antimony possess a rich oxide chemistry. Compounds Sb_2O_3;[5] α-[6] and β-Sb_2O_4[7] (low- and high-temperature forms, respectively), and $Sb_2O_{4.35}$ (Sb_6O_{13})[8] have been thoroughly characterized. The transition of α- to β-Sb_2O_4 is displacive and is reported to occur at 933–935 °C.[7] Both oxides have been structurally characterized.[6,7] There has been some confusion in the literature over the existence of isolated Sb_2O_5, but it appears now that materials identified as antimony pentoxide are in fact hydrates of antimonic acid of variable composition.[8]

In the course of our own investigations, we found that MoO_3 is marginally soluble in β-Sb_2O_4 and triggers the α-β transition at a lower temperature. In an effort to understand the structural role of Mo in this material, we have undertaken a powder neutron diffraction and Mo K-edge extended X-ray absorption fine structure (EXAFS) analysis of a sample of Mo-doped Sb_2O_4. Results of these and other (i.e., thermal analysis and Raman) investigations are reported herein.

Experimental Section

Materials and Methods. Sources of Sb for sample preparation were stabilized "Sb_2O_5" sol from Nalco or ultrapure Sb_2O_4 (Alfa Products). Sources for Mo were reagent grade MoO_3 powder or ammonium molybdate. Preparation of samples consisted of either coprecipitating the Sb sol with a solution of ammonium molybdate, followed by gradual evaporation and denitrification or grinding the oxides together prior to firing. In the work presented here, no differences between materials prepared by the two methods were discernible.

The X-ray absorption experiments were performed on thin layers of the sample that were prepared by first grinding the microcrystalline compound to a fine powder and then mixing the powder with a butyl acetate/acetone cement (Devcon Duco cement) thinned with acetone. The resulting slurry was uniformly spread on pure aluminum foil ($^1/_2$ mil thick) and air-dried. Several layers were stacked in order to obtain a sufficient concentration and an optimal change in the X-ray absorption coefficient across the Mo K-edge energy threshold.

Neutron Diffraction Measurements. Time-of-flight neutron diffraction data for a sample of Mo-doped (1.5%) Sb_2O_4 were collected at ambient temperature and pressure at Argonne National Laboratory with the IPNS (Intense Pulsed Neutron Source) on the special environment powder diffractometer. Data from the backscattering detectors (2θ = 150°) were used in the refinement, as these are the highest resolution data available from the instrument. The sample was contained within a $^1/_2$-in. diameter seamless vanadium tube, capped at both ends with aluminum plugs. Details of the instrument and the data collection and data analysis software package have been previously published.[9] Analysis of the data was performed with a Rietveld-profile least-squares program adapted for time-of-flight neutron data. Starting parameters for the least-squares process were taken from a single-crystal study of β-Sb_2O_4.[7] In the initial refinements, only nonmodel parameters were allowed to vary. In the final least-squares cycles, all parameters were allowed to vary, including the scale factor, profile (3), absorption, cell (4), and background parameters (5), as well as all fractional atomic coordinates (7) and isotropic temperature factors (2). The Sb atoms were constrained to lie on symmetry elements as in the X-ray model. The isotropic temperature factors of the two antimony atoms were constrained to be identical. The oxygen thermal parameters were handled in the same fashion. The occupancy factors of the antimony atoms and oxygen atoms were also varied in separate refinements. The occupancies of the O atoms are 1.01 (2) and 0.99 (2). In one analysis, a Mo atom was placed into an interstitial hole ($^1/_2$, 0, $^1/_2$; this is one site along a line of Sb^{III} lone-pair-electron density: $^1/_2$, 0, z) and its occupancy fixed at 0.015. The occupancies of the metal atoms were allowed to vary, and the refinement converged to yield values of 0.483 (8) and 0.504 (10) for Sb^{III} and Sb^{V}, respectively. Although the 0.483 value is only marginally different from full occupancy (0.50), it is the only occupancy factor to differ by more than 2 standard deviations from the value expected for a fully occupied site. The agreement factors for this analysis were R_{prof} = 0.044, R_{wprof} = 0.059, R_{nucl} = 0.035. Figure 1 displays the diffraction data, calculated plot, and difference curve. The fit between the diffraction data and calculated plot is excellent as evidenced by the magnitude of the difference plot. A comparison of the peak shapes of the Bragg reflections to the instrument/moderator parameters indicates that the sample contribution to peak broadening is negligible. This indicates that the sample consists of large, well-formed crystals with a small mosaic spread, which allows maximal use of the instrumental resolution (approximately 0.3%).[9] The results of the Rietveld analysis are therefore expected to be very accurate. Examination of the diffractogram gives no evidence of addi-

(1) (a) Grasselli, R. K.; Burrington, J. D. *Adv. Catal.* **1981**, *30*, 133. (b) Keulks, G. W.; Krenze, L. D.; Notormann, T. M. *Adv. Catal.* **1978**, *27*, 183. (c) Bielan'ki, A.; Huber, J. *Catal. Rev.—Sci. Eng.* **1979**, *19*, 1. (d) Cullis, C. F.; Hucknall, D. J. *Spec. Period. Rep.: Catalysis* **1983**, *5*, 273.
(2) Parmentier, M.; Courtois, A.; Gleitzer, C. *Bull. Soc. Chim. Fr.* **1974**, 75.
(3) Laarif, A.; Hewat, A.; Theobald, F.; Vivier, H. *J. Appl. Crystallogr.* **1983**, *16*, 143.
(4) Parmentier, M.; Gleitzer, C.; Tilley, R. J. D. *J. Solid State Chem.* **1980**, *31*, 305.
(5) Usov, Y. N.; Bolotov, I. M.; Kuvshinova, N. I.; Kitaev, V. I. *Neftekhimiya* **1975**, *15*, 242.
(6) Skapski, A. C.; Rogers, D. *J. Chem. Soc., Chem. Commun.* **1965**, 611.
(7) Skapski, A. C.; Rogers, D. *Proc. Chem. Soc.* **1964**, 400.
(8) Steward, D. J.; Knop, O.; Ayasse, C. *Can. J. Chem.* **1972**, *50*, 690.
(9) (a) Hauman, J. R.; Daley, R. T.; Worlton, T. G.; Crawford, R. K. *IEEE Trans. Nucl. Sci.* **1982**, *NS-29*, 62. (b) Von Dreele, R. B.; Jorgensen, J. D.; Windsor, C. G. *J. Appl. Crystallogr.* **1982**, *15*, 581. (c) Jorgensen, J. D.; Faber, J. *Argonne Natl. Lab., [Rep.] ANL* **1983**, *ANL-82-80*.

0020-1669/85/1324-3370$01.50/0

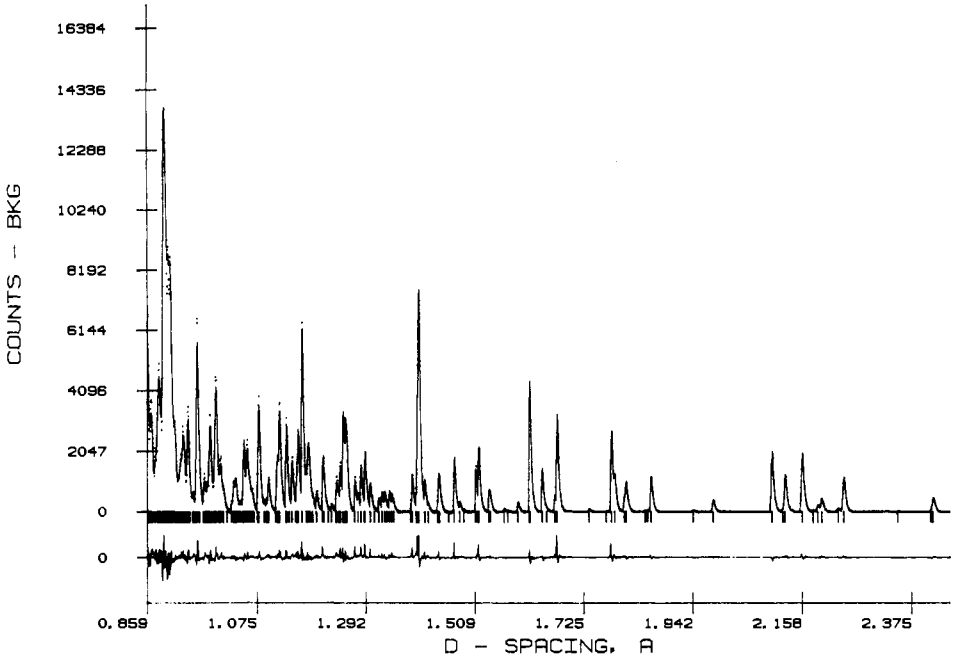

Figure 1. Powder neutron diffraction data (points) for Mo-doped β-Sb_2O_4. The calculated profile is indicated with a solid line, and a difference plot is given at the bottom of the figure. Vertical tick marks indicate locations of calculated Bragg reflections.

Table I. Rietveld Refinement Parameters for Mo-Doped β-Sb_2O_4

space group	$C2/c$, $Z = 4$	
cell consts	a	12.0571 (12) Å
	b	4.8335 (1) Å
	c	5.3838 (6) Å
	β	104.579 (5)°
	V	303.66 (7) Å^3
time-of-flight		6500 μs (d = 0.85 Å)
time-of-flight max		20000 μs (d = 2.42 Å)
bkgd params[a]	bk1	167 (53)
	bk2	−80 (70)
	bk3	24 (26)
	bk4	−4 (4)
	bk5	0 (1)
Gaussian half-width params[b]	$\sigma(0)$	187 (3)
	$\sigma(1)$	−93 (12)
	$\sigma(2)$	19 (1)
agreement factors	R_{prof}	0.044
(no. of points in profile 2701)	R_{wprof}	0.059
(no. of variables 25)	R_{exptl}	0.027
	R_{nucl}	0.035 (255 reflecns)

[a] The background is described by the function Ybk = bk1 + bk2-(exp(−bk3 d)) + bk4(exp(−bk5 d^2)). [b] The Gaussian portion of the profile function is given by $\sigma = \sigma(0) + \sigma(1)d + \sigma(2)d^2$.

tional phases (such as MoO_3). Scattering lengths used in the refinement are 0.695, 0.564, and 0.580 × 10^{-12} cm for Mo, Sb, and O, respectively. Details of the data collection are reported in Table I.

X-ray Absorption Measurements. Molybdenum K-edge X-ray absorption data for Mo-doped Sb_2O_4 were obtained at approximately 80 K in the transmission mode at the Stanford Synchrotron Radiation Laboratory (SSRL)[10] on beam line I-5.[11] The X-ray absorption data, in the form ln (I_0/I) vs. incident photon energy, were recorded with an integration time of 2 s/point by constant time accumulation for the incident (I_0) and transmitted (I) beam intensities. The photon energy was scanned from about 200 eV below to about 1000 eV above the Mo K-photoabsorption edge (19 999.5 eV)[12] at discrete monochromator steps corresponding to approximately constant k (photoelectron wave vector) increments. The monochromator steps ranged from 0.5 eV/point at the Mo K-edge to 4 eV/point at the end of each scan. Two spectra of equal length (355 points) were averaged.

The EXAFS data reduction[13] (including background removal and Fourier processing) and curve fitting were performed as described elsewhere.[14] The raw (averaged) Mo K-edge X-ray absorption data, ln

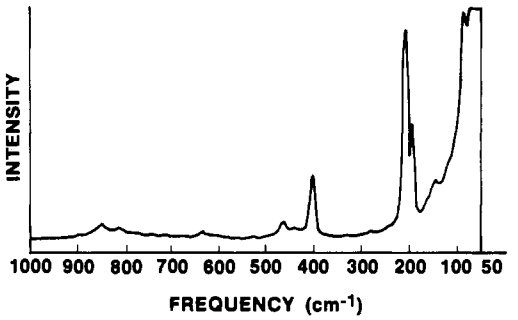

Figure 2. Raman spectrum of Mo-doped β-Sb_2O_4.

(10) SSRL utilizes the synchrotron radiation obtained from the dedicated operation of the Stanford Positron Electron Annihilator Ring (SPEAR) at the Stanford Linear Accelerator Center (SLAC). SPEAR is operated at ca. 3 GeV with between 30 and 70 mA of electron-beam current.

(11) The white synchrotron radiation from SPEAR was monochromated with two monolithic silicon ⟨220⟩ crystals. The monochromator was slightly detuned to reduce the harmonic content of the beam. The incident (I_0) and transmitted (I) beam intensities were monitored by flow-type ionization chambers using argon as the detecting gas in both chambers. The energy resolution at the molybdenum K-edge was ca. 5 eV. The beam size at the sample was ca. 1.5 × 17 mm^2.

(12) Bearden, J. A.; Burr, A. F. *Rev. Mod. Phys.* **1967**, *39*, 125.

(13) (a) For conversion to k (Å^{-1}) space ($k = [(2m/\hbar^2)(E - E_0^{exptl})]^{1/2}$), the experimental energy threshold (E_0^{exptl}) was chosen at 20011 eV. The edge position energy (E_0^{P}, the photon energy at half-height of the edge jump) was determined to be 20007.7 eV. After conversion to k space, the data were multiplied by k and the background was removed by using five sets (2.79 Å^{-1} each) of cubic spline functions. The EXAFS was normalized by dividing by the edge jump (0.033) and was also corrected for the falloff in the absorption cross section according to[13b] $\mu_0/\rho = C\lambda^3 - D\lambda^4$. Here μ_0/ρ is the mass absorption coefficient, λ is the wavelength of the incident X-radiation, and the parameters C and D for molybdenum are[13c] 555 and 336, respectively. (b) Victoreen, J. A. *J. Appl. Phys.* **1948**, *19*, 855. (c) Macgillavry, C. H., Rieck, G. D., Lonsdale, K., Eds. "International Tables for X-ray Crystallography"; Kynoch Press: Birmingham, England, 1968; Vol. III, pp 171–173.

(14) (a) Teo, B.-K.; Antonio, M. R.; Averill, B. A. *J. Am. Chem. Soc.* **1983**, *105*, 3751. (b) Antonio, M. R.; Teo, B.-K.; Cleland, W. E.; Averill, B. A. *J. Am. Chem. Soc.* **1983**, *105*, 3477. (c) Teo, B.-K.; Antonio, M. R.; Coucouvanis, D.; Simhon, E. D.; Stremple, P. P. *J. Am. Chem. Soc.* **1983**, *105*, 5767. (d) Teo, B.-K.; Chen, H. S.; Wang, R.; Antonio, M. R. *J. Non-Cryst. Solids* **1983**, *58*, 249. (e) Bruck, M. A.; Korte, H.-J.; Bau, R.; Hadjiliadis, N.; Teo, B.-K. In "Platinum, Gold, and Other Metal Chemotherapeutic Agents: Chemistry and Biochemistry"; Lippard, S. J., Ed.; American Chemical Society: Washington, DC, 1983; ACS Symp. Ser. No. 209, pp 245–262. (f) Teo, B.-K. In "EXAFS Spectroscopy: Techniques and Applications"; Teo, B.-K., Joy, D. C., Eds.; Plenum Press: New York, 1981; pp 13–58. (g) Lee, P. A.; Citrin, P. H.; Eisenberger, P.; Kincaid, B. M. *Rev. Mod. Phys.* **1981**, *53*, 769.

(I_0/I) vs. E (eV), and the background-subtracted Mo EXAFS spectrum, $k(\chi(k))$ vs. k (Å^{-1}), for Mo-doped Sb_2O_4 are shown as supplementary material.

Physical Measurements. Samples were also examined by scanning-electron microscopy (SEM) with a Cambridge Instruments CAM SCAN, equipped with a Kevex energy dispersive X-ray (EDX) analyzer. Examination of all samples revealed that all phases present consisted of large (30 μm) well-formed platelike crystals. EDX analysis (non-first-row elements) of the sample used in the neutron diffraction and EXAFS experiments indicated that the crystals were mostly Sb containing with a trace of Mo (1–2%). Similar analyses of samples with much higher concentrations of Mo revealed the presence of two crystalline morphologies (confirmed via powder X-ray diffraction (XRD) as MoO_3 and β-Sb_2O_4). The solubility of Mo in β-Sb_2O_4 was determined in the following manner: A sample consisting of 70 mol % Sb_2O_4 and 30 mol % MoO_3 was ground in a mortar and fired in a sealed, evacuated quartz tube at 850 °C for 80 h. At intervals of 24 h, the tubes were opened, the mixture was reground and sealed in fresh tubes, and the tubes were replaced in the oven. XRD analysis revealed the presence of two phases, MoO_3 and Sb_2O_4. SEM/EDX analysis of the β-Sb_2O_4 crystallites yielded $1^1/_2$ and $98^1/_2$ mol % for Mo and Sb (metals only), respectively.

The Raman spectrum of Mo-doped β-Sb_2O_4 was recorded in the 50–1000-cm^{-1} region at ambient temperature and is shown in Figure 2. The spectrum was recorded on a SPEX Ramalog equipped with a 0.85-μm Czerny–Turner double monochromator, an RCA C31034 cooled photomultiplier, and a Spectra-Physics 165 Ar ion laser. In order to minimize possible sample damage, ca. 50 mW of power was used (5145-Å line). Spectra were recorded with a slit width of ca. 7 cm^{-1}. Wavelengths are expected to be accurate to approximately 3 cm^{-1}.

Differential thermal analysis (DTA) and differential scanning calorimetry (DSC) were performed with a Du Pont 1090 thermal analyzer. The data were recorded from ambient temperature to 1000 °C, in air and in N_2.

Results and Discussion

Thermal Analyses. We have found that doping with Mo decreases the α–β transition of Sb_2O_4 from 934 to 825 °C. DTA of a MoO_3/Sb_2O_4 mixture reveals a small endotherm that begins at approximately 800 °C.

We have also found that thermal dehydration of commercially available "Sb sol" follows a different pathway from that for the thermal dehydration of a material identified as antimony pentoxide (but is most probably hydrated antimonic acid). Steward et al.[8] have made a detailed study of the thermal dehydration of antimonic acid and have found that materials of variable stoichiometry result until a temperature of 650 °C is reached and $Sb_2O_{4.35}$ is formed. In contrast to this, thermal treatment of commercial "Sb sol" at 425 °C produces exclusively α-Sb_2O_4. This latter observation coincides with that of Berry et al.,[15] who observed the production of α-Sb_2O_4 upon thermal treatment of antimony oxide nitrate hydroxide ($Sb_4O_4(OH)_2(NO_3)_2$). This latter material results from the reaction of antimony metal with nitric acid. These observations corroborate assertions in the literature[8,15] that products of calcination of antimony oxides are very dependent upon chemical processes that occur during the decomposition of the initial material.

The maximum solubility of Mo in antimony oxide has been determined to be $1^1/_2$ mol % (normalized to 100% metals only). This maximum solubility is difficult to achieve under routine synthesis conditions. When a mixture of Sb_2O_4 and excess MoO_3 is fired in an open container near the α–β transition temperature, a green melt is formed from which MoO_3 sublimes. When the limit of Mo solubility in Sb_2O_4 is reached, the yellow-tan solid β-Sb_2O_4 (Mo-doped) is observed. MoO_3 can also sublime from the MoO_3–Sb_2O_4 solid solution. Consequently, the maximum solubility of Mo in antimony oxide was determined by analysis of materials synthesized in sealed tube experiments.

Powder Neutron Diffraction Structure Description. The structure of β-Sb_2O_4 has been described previously on the basis of a single-crystal X-ray diffraction analysis.[7] The powder neutron diffraction results described herein corroborate this work, although the inherently greater sensitivity of neutrons to oxygen atom positions results in more accurate Sb–O bond lengths and angles.

(15) Berry, F. J.; Brett, M. *Inorg. Chim. Acta* **1984**, *83*, 167.

Table II. Final Positional and Thermal Parameters and Selected Distances (Å) and Angles (deg) in Mo-Doped β-Sb_2O_4, in Addition to Bond Distances (Å) for α-Sb_2O_4 for Comparison

A. Fractional Coordinates and Isotropic Temperature Factors

atom	10^4x	10^4y	10^4z	B_{iso},[b] Å^2	occupancy
Sb(1)[a]	5000	2838 (6)	7500	0.01 (8)	0.483 (8)
Sb(2)[a]	7500	2500	5000	0.01 (8)	0.505 (10)
O(1)	6918 (2)	523 (4)	1744 (4)	0.16 (10)	1.01 (1)
O(2)	4065 (2)	5877 (4)	5347 (3)	0.16 (10)	0.99 (1)

B. Coordination about Sb^V (Octahedral)[c]

Sb–O(1)	1.968 (1)	(1.958)	O(1)–Sb–O(1)′	88.47 (3)	(88.7)
Sb–O(1)′	1.957 (1)	(1.956)	O(1)–Sb–O(2)	95.12 (3)	(95.7)
Sb–O(2)	2.008 (1)	(1.990)	O(1)–Sb–O(2)	89.50 (5)	(89.8)
av	1.978				

C. Coordination about Sb^{III}

Sb–O(2)	2.208 (2)	(2.218)	O(2)–Sb–O(2)	147.31 (12)	(148.1)
Sb–O(2)′	2.029 (2)	(2.032)	O(2)–Sb–O(2)′	87.24 (10)	(87.9)

D. Distances about the Sb Atoms in α-Sb_2O_4[d]

	Sb^V		
Sb–O(1)	1.94	Sb–O(3)′	1.94
Sb–O(2)	1.98	Sb–O(4)	2.08
Sb–O(2)′	2.00	av	1.98
Sb–O(3)	1.92		
	Sb^{III}		
Sb–O(1)	2.30	Sb–O(4)	2.01
Sb–O(1)′	2.03	Sb–O(4)′	2.22

[a] Sb^V is constrained to lie on a center of symmetry; all trans angles are 180°. Sb^{III} is constrained to lie on a 2-fold axis. [b] The metal and oxygen atoms were constrained to have identical temperature factors, respectively. [c] Values from an earlier X-ray diffraction experiment[7] are shown in parentheses. [d] Values taken from ref 25.

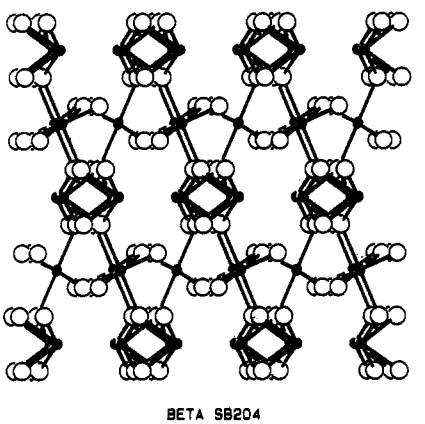

Figure 3. ORTEP diagram of β-Sb_2O_4, showing several unit cells with the [001] direction toward the viewer. The Sb atoms are represented by solid circles and the O atoms by open circles. Note the open channels perpendicular to the [001] face. As the Sb^{III} lone pairs are believed to occupy this space in the lattice, these channels represent regions of high electron density.

Final positional parameters and selected distances and angles are listed in Table II. The structure consists of corrugated layers of corner-linked SbO_6 octahedra (Sb^V) separated by sheets of SbO_4 polyhedra (Sb^{III}). The Sb^V atoms lie on a crystallographic inversion center, and the octahedron of O atoms is very symmetrically displaced about the metal atom. In contrast to this, the ligating oxygen atoms are very asymmetrically disposed about the Sb^{III} atoms, which are constrained to lie on a crystallographic 2-fold axis. This asymmetry is undoubtedly due to the presence of the Sb^{III} lone electron pair. The coordination about these Sb atoms can be envisioned as octahedral with two ligands removed to accommodate the lone pair. The remaining oxide ligands are then bent away from the lone pair, leading to the observed distorted oxygen environment. The [001] face of the structure is displayed in Figure 3. The Sb^{III} lone pairs can be seen as lining up to form channels (crystallographic direction: $^1/_2$, 0, z) of electron density

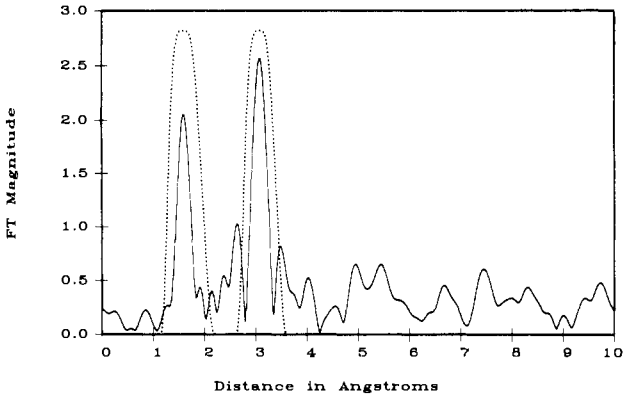

Figure 4. Fourier transform (solid curve) of the Mo K-edge EXAFS $k(\chi(k))$ vs. k and filtering windows (dotted curves) for Mo-doped Sb_2O_4.

perpendicular to the [001] face.

At one position along this line ($^1/_2$, 0, $^1/_2$), inserting a Mo atom results in a symmetric $Mo-O_4$ environment with almost equal (2.30 Å) Mo–O distances. The close approach of two Sb^{III} atoms to any site along the $^1/_2$, 0, z channel requires the simultaneous absence of both upon Mo^{VI} insertion (this would also satisfy charge balance requirements). Thus a $1^1/_2$% Mo interstitial occupancy would dictate a 97% Sb^{III} occupancy. This possibility was tested in a Rietveld refinement, and the occupancy of the Sb^{III} was found to be 96.6 (16)%. This result is statistically significant and is consistent with Mo atoms located interstitially within the β-Sb_2O_4 structure and a concurrent vacancy of 3% of the Sb^{III} sites. The next nearest Sb atoms (2) are 3.25 Å distant from ($^1/_2$, 0, $^1/_2$).

Raman Spectra Interpretation. The spectrum of 1% Mo-doped Sb_2O_4 (Figure 2) is very similar to that of undoped β-Sb_2O_4 reported by Cody et al.[16] Only slight differences in the band frequencies and intensities (principally in the lattice vibration region) are observed. Since there was no indication of sample damage due to laser heating, these differences cannot be attributed to thermal effects. It is reasonable to assume that site substitution of Sb by Mo would lead to more dramatic vibrational spectral changes than those observed. The differences documented herein are more in line with spectral perturbations expected for interstitial insertion of Mo into the β-Sb_2O_4 matrix. However, because of the low Mo-dopant level, the Raman technique cannot be used to unambiguously distinguish between site substitution and interstitial insertion. The possibility of a 1% MoO_3/99% Sb_2O_4 mixture can, however, be excluded on the basis of the Raman data. MoO_3 is a very strong scatterer, and observation of a 1% mixture of MoO_3 is easily within reach of the Raman experiment. As a check on this, a sample consisting of a mixture of MoO_3 and Sb_2O_4 (1% and 99%, respectively) was prepared at room temperature and the Raman spectrum of this mixture clearly showed the presence of MoO_3, in contrast to the spectrum of the Mo-doped antimony oxide. Additional evidence of the novel phase of β-Sb_2O_4 with Mo incorporation is found in the color of the material, which is yellow-tan, whereas pure β-Sb_2O_4 is white.

Mo K-Edge EXAFS Data. Because of the low Mo (1.5 mol % metal) content of the sample, it was not possible to unequivocally assign the Mo atom position in the crystal structure from the diffraction or vibrational data. An advantage of EXAFS spectroscopy over neutron diffraction methods is that EXAFS is an element-specific technique that is capable of probing the local structure around an X-ray-absorbing atom, regardless of the physical state of the sample. Thus, Mo K-edge EXAFS data were collected for the Mo-doped Sb_2O_4 sample in order to determine the structure in the immediate vicinity of the Mo atoms.

The Fourier transform of the normalized Mo EXAFS data, $k\chi(k)$ vs. k, for Mo-doped Sb_2O_4 exhibits two principal peaks at 1.61 and 3.07 Å (before phase-shift correction), which are assigned to Mo–O and Mo–Sb backscatterings, respectively (solid curve,

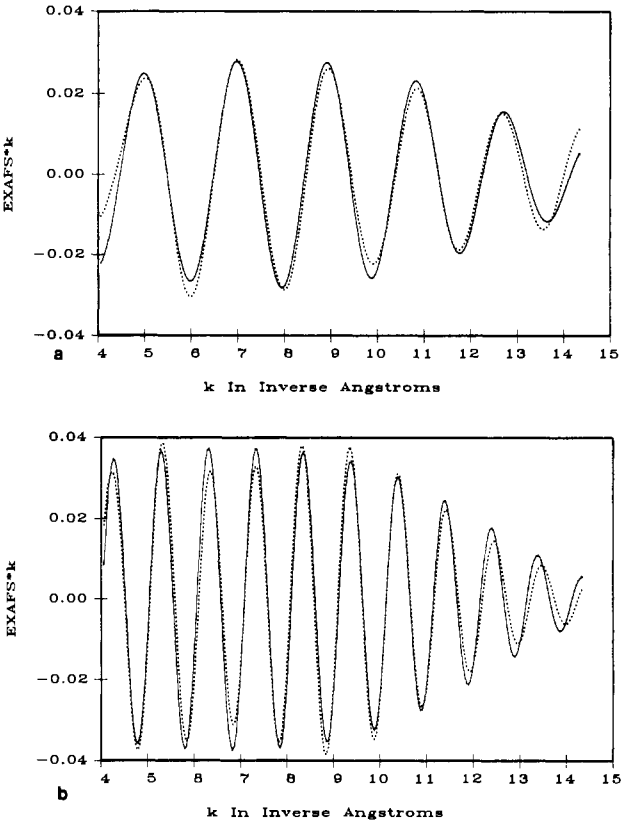

Figure 5. Fourier-filtered Mo K-edge EXAFS $k(\chi(k))$ vs. k (solid curves) and the nonlinear least-squares best fits (dotted curves), based on theoretical functions, to the filtered EXAFS of Mo-doped Sb_2O_4 for the (a) Mo–O and (b) Mo–Sb backscattering terms.

Figure 4). The two weaker peaks at 2.64 and 3.50 Å (uncorrected), which are on the low- and high-r side, respectively, of the Mo–Sb peak are presumably due to a combination of Fourier truncation error, residual background noise, and the shape of the Sb backscattering amplitude function. In k space, the Sb amplitude shows[17a] two peaks at ca. 3.5 and 11.0 $Å^{-1}$ and one valley at ca. 7 $Å^{-1}$. This particular shape of the Sb backscattering amplitude envelope may lead to the introduction of an aliased peak in the Fourier transform of these Mo EXAFS data.[17a] Alternatively, these two weak peaks might be interpreted as additional Mo–Sb (and/or Mo–O) backscatterings (the low dopant level precludes any Mo–Mo backscatterings). However, the apparent signal-to-noise ratio of the data set and the variability in the peak positions and magnitudes with different background removal treatments support the former interpretation.

For the purpose of curve fitting, the contributions of the Mo–O and Mo–Sb peaks in the Fourier transform of Mo-doped Sb_2O_4 (solid curve, Figure 4) were isolated from the distance space (Å) with two window functions (dashed curves, Figure 4) and back-transformed to k ($Å^{-1}$) space. The resulting Fourier-filtered EXAFS data, $k(\chi(k))$ vs. k, for the Mo–O and Mo–Sb backscatterings are shown in Figure 5a,b (solid curves), respectively.

A nonlinear least-squares curve-fitting technique[14,17] was used to fit the Fourier-filtered EXAFS data with a semiempirical formulation of the EXAFS phenomenon based on short-range, single-electron scattering theory:[18]

$$k(\chi(k)) = \sum B_j(F_j(k_j))(\exp[-2r_j/\lambda(k_j)]) \times (\exp[-2\sigma_j^2 k_j^2])r_j^{-2} \sin(2k_j r_j + \phi_j(k_j)) \quad (1)$$

(16) Cody, C. A.; Dicarlo, L.; Dalmington, R. K. *Inorg. Chem.* **1979**, *18*, 1572.

(17) (a) Teo, B.-K.; Lee, P. A. *J. Am. Chem. Soc.* **1979**, *101*, 2815. (b) Marquardt, D. W. *J. Soc. Ind. Appl. Math.* **1963**, *11*, 431. (c) The nonlinear least-squares parameter refinements were based upon the minimization of the sum of squares of the residuals, $\sum^2 = \sum[k_i(\chi(k)_i - Y(k)_i)]^2$. $Y(k)$ and $\chi(k)$ are the calculated and the observed EXAFS, respectively, and i runs through all the data points.

Table III. Least-Squares-Refined Interatomic Distances (r), Debye–Waller Factors (σ), Coordination Numbers (N), Energy Threshold Differences (ΔE_0^P), Scale Factors (B), and Mean-Free-Path Parameters (η) for the Mo K-edge Transmission EXAFS Data for Mo-Doped Sb_2O_4[a]

	Mo–O			Mo–Sb	
	best fit			best fit	
param	$\Sigma^2 = 0.0018$	$\Sigma^2 = 0.0059$	FABM	$\Sigma^2 = 0.0025$	FABM
r, Å	2.016 (27)	1.980 (31)	1.957 (21)	3.357 (25)	3.303 (38)
ΔE_0^P, eV[b]	16.50	2.27	0.54[c]	−5.98	−12.40[c]
σ, Å	0.001 (50)	0.044 (40)	0.038 (23)[c]	0.091 (12)	0.068 (21)[c]
B	1.512	3.468	1.825–3.184	5.296	3.020
N	3.1 (6)	5.2 (15)	3.0–5.2	1.5 (7)	1.3 (8)
η, Å	11.47	20.90		7.24	

[a] Estimated standard deviations are given in parentheses. [b] Standardized energy threshold differences ΔE_0^P were obtained according to $\Delta E_0^P = E_0 + E_0^{exptl} - E_0^P$. Here ΔE_0 was the least-squares-refined energy threshold difference, E_0^{exptl} was the experimentally chosen threshold energy, and E_0^P was the edge-position energy.[13a] [c] These parameters were obtained from the EXAFS data for the model compound MoO_3 and were transferred to the data for Mo-doped Sb_2O_4.

Here, $F_j(k_j)$ and $\phi_j(k_j)$ are the theoretical backscattering and phase functions,[19] respectively, σ_j is the Debye–Waller factor, and the scale factor B_j is equal to S_jN_j, where S_j is the amplitude reduction factor and N_j is the number of neighboring atoms of the jth type at a distance r_j away from the X-ray absorbing atom. The term $\exp[-2r_j/\lambda(k)]$ accounts for the lifetime of the core hole and inelastic scattering losses. The electron mean free path ($\lambda(k)$) was approximated[20] by $\lambda(k) = k^2/\eta$, where η is the mean-free-path parameter.

The back-transformed, filtered Mo EXAFS data $k\chi(k)$ for both the oxygen and antimony backscatterings were fit with a single-term formulation of the EXAFS effect, j = O and Sb (eq 1), respectively. Five parameters were refined in the nonlinear least-squares curve fitting: the scale factor B, the Debye–Waller factor σ, the interatomic distance r, the energy threshold difference ΔE_0, and the mean-free-path parameter η. Figure 5a,b shows the best fits using theoretical functions (dashed curves) with the EXAFS formulation and the Fourier-filtered Mo–O and Mo–Sb data (solid curves), respectively, for Mo-doped Sb_2O_4 over the range $4 \le k \le 14.5$ Å^{-1}. It is evident from Figure 5 that the single-term fits to the Mo EXAFS are satisfactory, as judged by the relative goodness of the fits[17c] ($\sum^2 = 0.0018$ and 0.0025 for the Mo–O and Mo–Sb terms, respectively).

The best-fit parameters obtained from the nonlinear least-squares refinements are tabulated in Table III; estimated standard deviations are also given (in parentheses) for all interatomic distances and Debye–Waller factors. These fitting-error estimates are independent of systematic errors, such as in background removal and Fourier filtering, that could give rise to additional uncertainties. An examination of the error estimates and parameter correlations obtained from the single-term (Mo–O) stepwise curve-fitting procedure[14a] to the Mo $k(\chi(k))$ vs. k data for Mo-doped Sb_2O_4 revealed another minimum in the residual $\sum^2$ surface. Although the goodness-of-fit ($\sum^2 = 0.0059$) for this minimum is some 3 times worse than that ($\sum^2 = 0.0018$) for the best-fit minimum, we are unable to dismiss the resulting structural parameters (Table III) on the grounds of an unrealistic and/or artificial false convergence. The residual function for the Mo–Sb term was smooth and unimodal.

In order to ascertain the exact nature of the oxygen coordination and to determine the number of O and Sb neighbors around Mo, the fine adjustment based on models (FABM) method[14a-e] was applied to these data by using the Mo EXAFS of the model compound MoO_3 (measured and analyzed in a similar fashion) for the Mo–O and Mo–Sb interactions in Mo-doped Sb_2O_4. As described elsewhere,[14a] the number of O and Sb neighbors was calculated by dividing the scale factors (Table III) by the amplitude reduction factors obtained from the B vs. σ correlation curves of MoO_3 (available as supplementary material). The interatomic distance adjustments were determined with the Mo–O and Mo–Mo characteristic energy threshold differences for MoO_3 (Table III) and the slopes of the ΔE_0^P vs. Δr correlation curves (supplementary material), as also described elsewhere.[14a] The FABM results are tabulated in Table III.

The FABM treatment of the Mo K-edge EXAFS data for Mo-doped Sb_2O_4 indicates that the Mo atom has between three and five oxygen atoms at 1.96 (2) Å as nearest neighbors. The EXAFS determined interatomic distance (1.96 Å) is larger than expected for typical four-coordinate Mo^{6+}–O distances of ca. 1.75–1.80 Å.[21] Nevertheless, it is possible that steric constraints at the Mo site imposed by the β-Sb_2O_4 matrix account for the larger than average length of the Mo–O bonds.

In the absence of model compounds with Sb neighbors around Mo, the fine adjustments to the best-fit Mo–Sb data for Mo-doped Sb_2O_4 were calculated by using the Mo–Mo parameters obtained from the EXAFS spectrum of MoO_3. The results are therefore only accurate inasmuch as the Mo–Mo model parameters mimic those of the Mo–Sb backscattering term. The similarity between the parameters (Table I-S, supplementary material) and curvature (Figures III-S and IV-S, supplementary material) of the $\sum^2$ minimum surface for the Mo–Sb and Mo–O terms of Mo-doped Sb_2O_4, on the one hand, and those for the Mo–Mo and Mo–O terms of MoO_3, on the other, respectively, supports the use of MoO_3 as a good model compound. The FABM results for Mo-doped Sb_2O_4 (Table III) indicate that the Mo atoms have one or two Sb atoms at 3.30 (4) Å as second nearest neighbors.

Given the present model compound and the data set employed in our EXAFS analysis, it is not possible to unequivocally determine the exact number of both metal neighbors (one or two antimony atoms) and oxygen neighbors (three–five oxygen atoms). In fact, it is generally recognized that coordination numbers are significantly more difficult to determine by EXAFS spectroscopy than are interatomic distances.

(18) (a) Sayers, D. E.; Lytle, F. W.; Stern, E. A. In "Advances in X-ray Analysis"; Henke, B. L., Newkirk, J. B., Mallett, R. G., Eds.; Plenum Press: New York, 1970; Vol. 13, pp 248–271. (b) Sayers, D. E.; Stern, E. A.; Lytle, F. W. *Phys. Rev. Lett.* **1971**, *27*, 1204. (c) Stern, E. A. *Phys. Rev. B: Solid State* **1974**, *10*, 3027. (d) Lytle, F. W.; Sayers, D. E.; Stern, E. A. *Phys. Rev. B: Solid State* **1975**, *11*, 4825. (e) Stern, E. A.; Sayers, D. E.; Lytle, F. W. *Phys. Rev. B: Solid State* **1975**, *11*, 4836. (f) Ashley, C. A.; Doniach, S. *Phys. Rev. B: Solid State* **1975**, *11*, 1279. (g) Lee, P. A.; Pendry, J. B. *Phys. Rev. B: Solid State* **1975**, *11*, 2795. (h) Kincaid, B. M.; Eisenberger, P. *Phys. Rev. Lett.* **1975**, *34*, 1361. (i) Lee, P. A.; Beni, G. *Phys. Rev. B: Solid State* **1977**, *15*, 2862.

(19) For each k value, the theoretical backscattering amplitude and phase functions for Sb (Z = 51) were obtained by a simple point-by-point weighted arithmetic average of the corresponding functions for Sn (Z = 50) and I (Z = 53). The theoretical values of the EXAFS functions $F(k)$ and $\phi(k)$, calculated by Teo and Lee (by using Herman–Skillman wave functions) at discrete intervals in k (Å^{-1}) space, were obtained from ref 17a: from Table VII for the central atom phase ϕ_{Mo}; from Table V for the backscattering phases ϕ_{Sn} and ϕ_I; and from Table IV for the backscattering amplitudes F_{Sn} and F_I. Oxygen phase ϕ and amplitude F functions were obtained from ref 20a: from Table II-S, supplementary material, for $\beta = 180°$.

(20) (a) Teo, B.-K. *J. Am. Chem. Soc.* **1981**, *103*, 3990. (b) Alberding, N.; Crozier, E. D. *Phys. Rev. B: Condens. Matter* **1983**, *27*, 3374.

(21) (a) Jeitschko, W.; Sleight, A. W.; McClellan, W. R.; Weiher, J. F. *Acta Crystallogr., Sect. B: Struct. Crystallogr. Cryst. Chem.* **1976**, *B32*, 1163. (b) Abrahams, S. C.; Reddy, J. M. *J. Chem. Phys.* **1965**, *43*, 2533. (c) Smith, G. W.; Ibers, J. A. *Acta Crystallogr.* **1965**, *19*, 269.

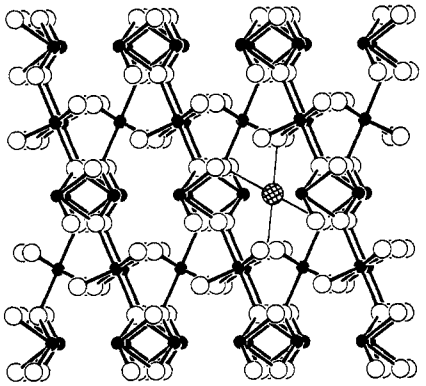

Figure 6. ORTEP of Mo-doped β-Sb_2O_4, showing several unit cells with the [001] direction toward the viewer. The Sb atoms are reprsented by solid spheres, the O atoms are represented by open spheres, and the lone Mo atom is represented as a crosshatched sphere. The two Sb atoms nearest the Mo atom (ca. 2.00 Å distant) have been removed.

Summary

There are numerous examples of elemental doping that induce phase changes in solid materials at temperatures below that normally observed. The reduction of the phase transition temperature observed in this work is the second reported for Sb_2O_4. Berry et al. have noted that 5% V in Sb_2O_4 lowers the α–β transition as well.[22] What is somewhat surprising is the small amount (ca. 1%) of Mo needed to effect the phase change and the limited solubility of Mo in the final phase. Perhaps the ease with which the phase change is triggered is more a reflection of the marginal difference in stability between the α and β forms of Sb_2O_4. Table II lists distances about the two types of antimony atoms in α-Sb_2O_4, and a comparison of these values with those of the β form reveals a small structural difference.

Although the diffraction and Raman data were not useful in directly identifying the environment of Mo in β-Sb_2O_4, the EXAFS data have been valuable in determining the Mo coordination environment. There are two possibilities for Mo incorporation into Sb_2O_4: interstitial insertion and antimony substitution. As to the latter possibility, the EXAFS-derived Mo–O distance (1.96 Å) matches the average Sb–O distance for the octahedral Sb^V site, whereas the coordination number (3–5) fits the asymmetric Sb^{III} site. Size considerations would seem to favor Mo octahedral substitution because Mo^{VI} and Sb^V are nearly the same size (effective ionic radii are 0.60 and 0.61 Å, respectively[23]). Also, there are numerous molybdenum oxides with octahedrally coordinated Mo atoms, although in many of these compounds the MoO_6 octahedra are asymmetric, not symmetric as for the Sb^V sites in β-Sb_2O_4. The simple oxides (MoO_3 and MoO_2[24]) and bismuth oxides ($Bi_2Mo_3O_{12}$ and Bi_2MoO_6[25]) offer examples of asymmetric oxygen environments surrounding Mo atoms. A major difference between Mo^{VI} and Sb^V is, of course, the absence and presence of 10 electrons on 5 d orbitals, respectively. From a chemistry standpoint then, a simple substitution of Mo^{VI} for Sb^V may not be warranted.

Alternately, substitution of Mo for the asymmetric Sb^{III} atom should ideally lead to different sets of Mo–O distances corresponding to the Sb–O (2.208 (2) and 2.029 (2) Å) distances. However, the Fourier transform of the Mo EXAFS data exhibits a single peak due to Mo–O backscattering. It is possible that substitution of a Mo atom for an Sb atom in this site could produce local distortions in the oxygen atom environment and lead to one type of Mo–O distance. It should be noted that, for each substitution of Mo^{VI} for one Sb^{III}, $1^1/_2$ oxygen vacancies could result (for $1^1/_2$% total Mo substitution, $2^1/_4$% oxygen vacancies) and that this was not borne out by the Rietveld analysis. Refinements of the diffraction data indicate that all oxygen sites are fully (100%) occupied. Alternatively, charge balance could be achieved by absence of a second Sb^{III} atom. The substitution of one Mo atom (scattering length 0.695) for two Sb atoms (scattering length 0.564) results in a scattering length not significantly different from that obtained for 100% Sb occupancy of the Sb^{III} sites (contrary to the diffraction data analysis).

As noted above, the Sb_2O_4 structure contains open channels (presumably containing Sb^{III} lone pairs) perpendicular to the [001] face. Insertion of Mo atoms in this channel (crystallographically located along the line $^1/_2$, 0, z) results in a coordination sphere of four oxygen atoms for the inserted Mo atom. The close approach of two Sb^{III} atoms necessitates their removal (assuming no oxygen vacancy, this is also dictated by charge balance considerations). The most symmetric site along this line is at ($^1/_2$, 0, $^1/_2$), which places the Mo atom 2.3 Å away from four O atoms. Local distortions that result in the contraction of these oxygen atoms toward the interstitial atom would yield a coordination environment consistent with the interpretation of the EXAFS data and also Rietveld refinements of the neutron diffraction data. On the basis of these results, we hypothesize that the Mo atom resides interstitially in β-Sb_2O_4, resulting in the observed 97% site occupancy of the Sb^{III} site. A drawing of Mo inserted into the β-Sb_2O_4 lattice is shown in Figure 6. Additional evidence for this interpretation is found in the second nearest-neighbor (Mo–Sb) distance (3.30 Å) from EXAFS data, which agrees well with the crystallographic calculation of 3.25 Å for the shortest Mo–Sb^V distance.

Acknowledgment. We are indebted to Dr. D. R. Sandstrom (Boeing Co.) and L. C. Glaeser (Sohio) for assistance with the X-ray absorption measurements, and we also thank Dr. S. Iyengar and M. Mittleman (Sohio) for technical assistance. SSRL is supported by the NSF through the Division of Materials Research and the NIH through the Biotechnology Resource Program in the Division of Research Resources in cooperation with the Department of Energy. We are also grateful to Dr. J. Jorgensen (Argonne) for his assistance with the time-of-flight neutron data collection. The authors acknowledge the U.S. Department of Energy for supporting the Intense Pulsed Neutron Source at Argonne as a national user's facility and the Standard Oil Co. (Sohio) for permission to publish this work.

Registry No. Sb_2O_4, 1332-81-6; Mo, 7439-98-7.

Supplementary Material Available: Figure I-S (raw X-ray absorption data in the form ln (I_0/I) vs. E (eV)), Figure II-S (background-subtracted and Fourier-filtered $k(\chi(k))$ vs. k (Å^{-1})), Figures III-S and IV-S (parameter correlations, B vs. σ and ΔE_0 vs. Δr, encountered in the nonlinear least-squares curve fitting to the filtered Mo EXAFS data of Mo-doped Sb_2O_4 and MoO_3), Table I-S (linear least-squares regression coefficients for the parameter correlations obtained from curve fitting), and Table II-S (raw neutron diffraction data for Mo-doped Sb_2O_4) (17 pages). Ordering information is given on any current masthead page.

(22) Berry, F. J.; Brett, M. E. *J. Chem. Soc., Dalton Trans.* **1984**, 985.
(23) Huheey, J. E. "Inorganic Chemistry"; Harper and Row: New York, 1972.
(24) Kihlborg, L. *Ark. Kemi* **1963**, *21*, 357.
(25) The structures of these materials have been discussed in numerous publications; definitive results are to be found in: (a) Van den Elzen, A. F.; Rieck, G. D. *Acta Crystallogr., Sect. B: Struct. Crystallogr. Cryst. Chem.* **1973**, *B29*, 2433, 2436. (b) Teller, R. G.; Brazdil, J. F.; Grasselli, R. K.; Jorgensen, J. D., *Acta Crystallogr.*, in press. (c) Teller, R. G; Brazdil, J. F.; Grasselli, R. K.; Kostiner, E., manuscript in preparation.